

**Hierarchical wrinkles and oscillatory cracks in metal films deposited on liquid stripes**Senjiang Yu,<sup>1</sup> Yadong Sun,<sup>2</sup> Xiaofei Zhang,<sup>2,\*</sup> Chenxi Lu,<sup>1</sup> Hong Zhou,<sup>2</sup> and Yong Ni<sup>3,†</sup><sup>1</sup>*Innovative Center for Advanced Materials (ICAM), Hangzhou Dianzi University, Hangzhou 310012, People's Republic of China*<sup>2</sup>*Department of Physics, China Jiliang University, Hangzhou 310018, People's Republic of China*<sup>3</sup>*CAS Key Laboratory of Mechanical Behavior and Design of Materials, Department of Modern Mechanics, University of Science and Technology of China, Hefei, Anhui 230026, People's Republic of China*

(Received 2 March 2019; published 20 June 2019)

Fascinating crack and wrinkle patterns driven by stresses are ubiquitous in natural and artificial systems. It is of great interest to control the morphologies of stress-driven patterns by using facile techniques. Here we report on the spontaneous formation of hierarchical wrinkles and oscillatory cracks in metal films deposited on liquid (or soft polymer) stripes. It is found that the metal film is under a tensile stress during deposition owing to the thermal expansion of the liquid substrate. As the film thickness is beyond a critical value, oscillatory cracks with sawtoothlike shapes form on the liquid stripes. The ratio of crack oscillation period to amplitude is independent of the stripe width and film material, which can be well explained by the “brittle adhesive joints” model. After deposition, the metal film is under a compressive stress, which is relieved by formation of various wrinkle patterns. Hierarchical wrinkles with changing wavelengths form near the stripe edge while labyrinth or wavy wrinkles form at the center. Energy analysis was adopted to explain the formation and evolution of the wrinkle patterns. This study could promote better understanding of the formations of crack and wrinkle patterns in constrained film structures and controllable fabrication of stress-driven patterns by prefabricating liquid (or soft polymer) interlayer arrays.

DOI: [10.1103/PhysRevE.99.062802](https://doi.org/10.1103/PhysRevE.99.062802)**I. INTRODUCTION**

Films and sheets floating on liquid surfaces are ubiquitous in natural and artificial systems such as tectonic plates, floating ices, milk skins, Langmuir-Blodgett films, membranes in animals and plants, etc. Recently, mechanical responses of elastic polymer sheets floating on liquid surfaces under loading have received a great deal of attention. Huang *et al.* reported radial wrinkles in a freely floating polystyrene film under the capillary force exerted by a drop of water placed on its surface [1]. Pocivavsek *et al.* reported the transition from sinusoidal wrinkles to localized folds in polymer sheets on liquid substrates by progressively increasing uniaxial compression [2]. Holmes and Crosby reported the wrinkle-to-fold transition in an elastic sheet floating on a surface of water when lifting at the sheet center by a spherical probe [3]. King *et al.* reported the wrinkle-to-crumple transition in an elastic sheet on a liquid drop by increasing drop curvature (i.e., surface tension) [4]. Paulsen *et al.* reported rich wrinkle and fold morphologies in a flexible annulus floating on a bath of water by exerting different tensions on the inner and outer rims [5].

The mechanical responses of brittle (metal, ice, crystal, etc.) films on liquid surfaces are also studied in a large number of recent investigations. Liu and Wuttig reported a creased growth morphology in square perylene crystals on an oil substrate [6]. Deng and Berry reported hierarchical wrinkles

in stiff metal films on a liquid meniscus [7]. Yu *et al.* reported similar hierarchical wrinkles in metal chromium films on circular silicone oil disks [8]. Compared with the polymer sheets, the brittle films are susceptible to fracture under a tensile stress or bending-induced ridge cracking under a large compressive stress. Cai *et al.* reported the spontaneous formation of parallel sinusoidal cracks in metal nickel films deposited on silicone oil substrates [9]. Some researchers reported peculiar square periodic cracks (also called interlocking finger cracks) in various metal films on silicone oil substrates [10,11]. Vella and Wettlaufer theoretically explained the formation of interlocking finger cracks observed in floating ices [12].

Although the mechanical responses of films and sheets on unlimited liquid surfaces have been extensively investigated in the past decade, the effect of geometric constraint of liquid substrate on film deformation is still an unsolved issue. Here we prefabricated controllable silicone oil stripes on glass substrates and then deposited metal films on the heterogeneous surfaces. The geometric constraint effect of silicone oil stripes ultimately leads to specific hierarchical wrinkles and oscillatory cracks. The cracks are driven by the tensile stress during film deposition while the wrinkles are caused by the compressive stress after film deposition. The period of oscillatory crack is precisely controlled by the stripe width, which can be well explained by the “brittle adhesive joints” model. The formation and evolution of wrinkle patterns are attributed to the competition between bending energy of film, thermal expansion energy of substrate, and surface energy applied on the metal film from the metal-glass interface to the metal-liquid interface. This technique can be developed to controllably fabricate various surface patterns via

\*zhangxf@cjl.u.edu.cn

†yni@ustc.edu.cn

prefabricating liquid stripe arrays by direct ink writing or other printing methods.

## II. EXPERIMENTAL DETAILS

### A. Preparation of silicone oil stripes

Silicone oil (Dow Corning) was used to construct the liquid stripes on glass slides with the sizes of  $\sim 20 \times 10 \text{ mm}^2$ . The coefficient of viscosity of silicone oil was varied from 10 to  $1 \times 10^6 \text{ cP}$  ( $1 \text{ cP} = 10^{-3} \text{ Pa s}$ ). It was found that the silicone oil with small viscosity coefficient would flow and spread on the glass surface during the film deposition, while it was hard to form narrow stripes with the silicone oil with large viscosity coefficient. Therefore, the coefficient of viscosity of silicone oil was fixed at  $5 \times 10^5 \text{ cP}$  in this study. First a needle was dipped into the bulk silicone oil and then pulled out. Some silicone oil would be attached to the needle tip to form a very small drop. Then another needle tip touched the small silicone oil drop and then was separated controllably. The silicone oil would become threadlike and its diameter was determined by the distance between these two needle tips. Finally the silicone oil filament was placed on the glass slide carefully to form silicone oil stripe with a certain width. The profiles of silicone oil stripes were detected by a stylus profiler (DektakXT, Bruker). The maximum silicone oil height generally increased with increasing stripe width, as shown in Supplemental Material Fig. S1 [13]. The average slope of silicone oil stripe (i.e., the ratio of maximum height to half width) was about  $0.06$ , which corresponds to an inclined angle of only  $3.4^\circ$ . The curvature of the film is very small and can be neglected in this study.

### B. Preparation of PDMS stripes

We also prepared elastic PDMS (polydimethylsiloxane, Dow Corning's Sylgard 184) stripes on glass slides. First liquid PDMS was synthesized by mixing the base and curing agent with 10:1 mass ratio. After degassing, the liquid PDMS was placed on a hot plate with  $100^\circ\text{C}$  for 5 min to form very viscous fluid. Then the PDMS stripes were prepared on glass slides by using the two-needle method as described above. Finally the sample was baked at  $100^\circ\text{C}$  for 2 h to crosslink the PDMS completely.

### C. Film deposition and characterization

Metal films were deposited on the silicone oil (or PDMS) stripes and glass surfaces simultaneously by direct current magnetron sputtering at room temperature. Various film materials including iron, copper, nickel, titanium, and cobalt were used in this study and they led to similar experimental results. All the metal targets had the same size of 60 mm in diameter and 3 mm in thickness. The target-to-substrate distance was about 80 mm. The chamber pressure was first pumped below  $2 \times 10^{-4} \text{ Pa}$  and then pure argon gas was filled into the chamber to keep the pressure of 0.5 Pa during sputtering. The deposition rates for all the metal films were fixed at  $\sim 0.25 \text{ nm/s}$ . The deposition time was varied from several seconds to tens of minutes, which was precisely controlled by a computer. Note that there exists a critical amount of deposited material to form a stable film (namely critical percolation point), under

which nonuniform networklike film can be observed [14,15]. Furthermore, the metal particles with large kinetic energy can penetrate deeper into the liquid with low viscosity [16]. However, the coefficient of viscosity of silicone oil in our experiment is large enough and no obvious percolated or networklike structure can be observed even if the nominal film thickness is less than 1 nm. Therefore, the critical percolation effect and penetration effect are not considered in this study. The surface morphologies were investigated by an optical microscopy (Olympus BX41) and an atomic force microscopy operated in tapping mode (AFM, Veeco Dimension 3100). The temperature variation of the sample surface after film deposition was measured by an infrared thermometer (Smart Sensor AR852B<sup>+</sup>).

## III. RESULTS AND DISCUSSION

### A. Hierarchical wrinkling of thinner films

Figures 1 and 2 show the typical morphologies of iron films with varied thicknesses deposited on silicone oil stripes with smaller and larger widths, respectively. We find that the films on glass surfaces remain flat while they are wrinkled on the silicone oil stripes. The wrinkle patterns are strongly dependent on the stripe width and film thickness. Generally, ordered straight wrinkles form near the stripe edge while labyrinthlike wrinkles appear at the center. The length of straight wrinkles near the edge  $L$  (i.e., the distance from the stripe edge to the end of straight wrinkles) increases successively with increasing film thickness, as shown in Fig. 3(a). For a given sample, the length  $L$  increases approximately linearly with increasing stripe width, as shown in Supplemental Material Fig. S2 [13].

Another interesting phenomenon shown in Figs. 1 and 2 is that the wrinkle wavelength increases with increasing distance from the stripe edge, namely  $x$ , leading to the formation of a characteristic hierarchical wrinkle pattern. Quantitative measurement shows that as the distance increases, the wrinkle wavelength increases quickly first, and then the growth speed slows down gradually, as shown in Fig. 3(b). The experimental data can be well fitted by a power law  $\lambda \propto x^n$  with the power exponent  $n = 0.46 \pm 0.03$ .

To detect more structural details of the hierarchical wrinkles, they were taken by the atomic force microscopy (AFM), as shown in Fig. 4(a). It is clear that the wrinkle amplitude also increases with increasing distance  $x$ . The optical and AFM images show that a shorter wrinkle is usually sandwiched by two longer wrinkles near the edge. Such a feature can be well verified by the cross-sectional profile (line 1) as shown in Fig. 4(b), where the tiny wrinkle (small amplitude) and strong wrinkle (large amplitude) alternately occur. When the distance from the edge increases, the tiny wrinkle disappears while the strong wrinkle is retained. That is to say, a pair of wrinkles (a tiny wrinkle and a strong wrinkle) merges into one wrinkle, which is the typical feature of hierarchical wrinkling [7,8].

It is now well known that the film deposition process will lead to an obvious temperature rise of the sample [7,8,17]. For the thicker film in our experiment ( $h = 450 \text{ nm}$ ), the temperature variation during deposition measured by the infrared thermometer was about 40 K. The thermal stress of the film

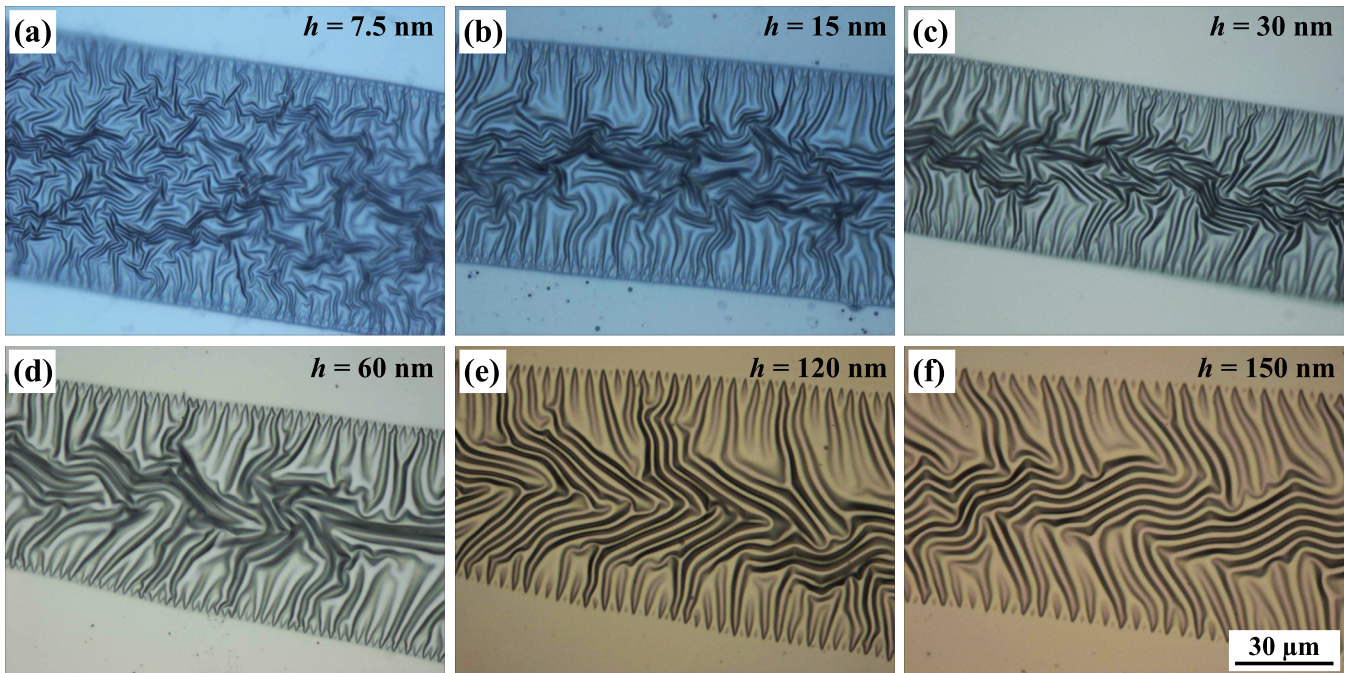


FIG. 1. Morphological evolution of wrinkle patterns with increasing film thickness (here it is iron) for narrower silicone oil stripes. All images have the same size of  $139 \times 104 \mu\text{m}^2$ .

can be calculated by  $\sigma_{th} = \frac{E_f(\alpha_s - \alpha_f)\Delta T}{1 - \nu_f}$ , where  $E$  is the elastic modulus,  $\nu$  is Poisson's ratio,  $\alpha$  is the thermal expansion coefficient,  $\Delta T$  is the temperature variation, the subscripts  $f$  and  $s$  refer to the film and substrate, respectively. For the iron-silicone oil system,  $E_f \approx 200 \text{ GPa}$ ,  $\nu_f \approx 0.3$ ,  $\alpha_f \approx 1.2 \times 10^{-5} \text{ K}^{-1}$ ,  $\alpha_s \approx 79 \times 10^{-5} \text{ K}^{-1}$ ,  $\Delta T \approx 40 \text{ K}$ , and then

the thermal stress of the film with  $h = 450 \text{ nm}$  can be estimated to be about  $8.9 \text{ GPa}$ . The corresponding thermal strain is about  $3.1 \times 10^{-2}$ . It is clear that the film under such tensile stress during deposition due to temperature rise is large enough to generate cracks while it can switch to a compressive stress after deposition due to temperature reduc-

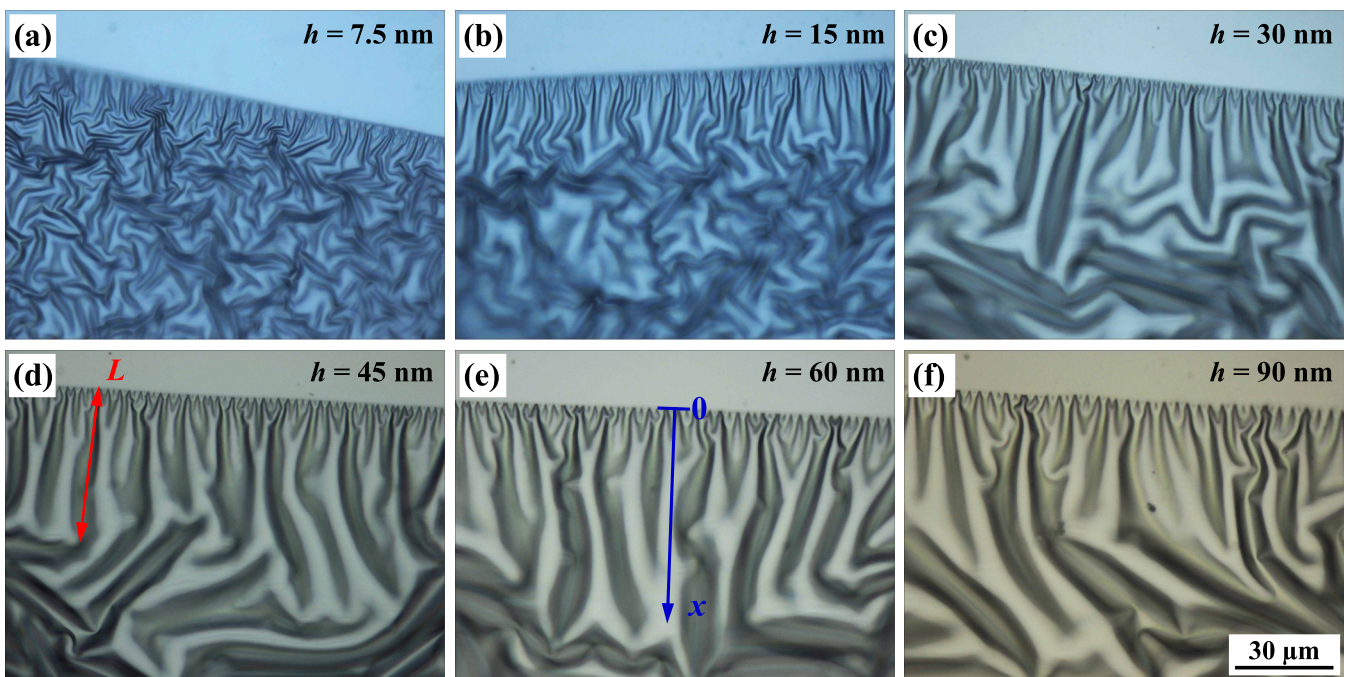


FIG. 2. Morphological evolution of hierarchical wrinkles with increasing iron film thickness for wider silicone oil stripes. The length of straight wrinkles at the stripe edge is denoted as  $L$ . The distance starting from the stripe edge is denoted as  $x$ . All images have the same size of  $139 \times 104 \mu\text{m}^2$ .

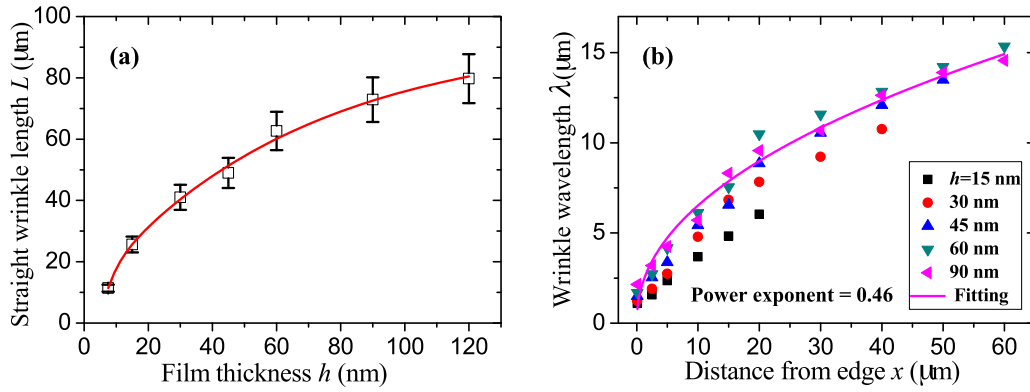


FIG. 3. (a) Evolution of the straight wrinkle length  $L$  with the film thickness  $h$ . The solid line is a guide to the eye. (b) Evolution of the wavelength of straight wrinkles  $\lambda$  with the distance  $x$  for varied film thicknesses. The solid line is a fit to the experimental data with a power law  $\lambda \propto x^n$  for  $h = 90$  nm.

tion and induce wrinkles. Note that the film thickness for crack initiation is smaller than 90 nm (see the next section) and thus the critical tensile stress for cracking is below 1.8 GPa. The critical compressive strain for wrinkle formation can be expressed as  $\epsilon_c = \frac{1}{4} \left( \frac{3E_s(1-\nu_f^2)}{E_f(1-\nu_c^2)} \right)^{2/3}$  [18,19]. For the current system, the “equivalent modulus” of silicone oil is not above 0.5 MPa (see below). The critical strain can be estimated to be about  $9.6 \times 10^{-5}$ , which is much smaller than the thermal

strain. Therefore, the wrinkles can be easily observed in our experiment, even for the very thin film sample.

Many previous works have investigated the wrinkle morphologies induced by various film impurities such as film edges, cracks, relief steps, and boundaries of different phases [18–22]. Bowden *et al.* have discussed the stress distribution near the impurity edge [18]. It shows that the stress near the free edge is quasiuniaxial and parallel to the edge, which is relieved by formation of straight wrinkles perpendicular to the edge. As the distance from the edge increases, the uniaxial stress will evolve into equibiaxial stress gradually, and thus labyrinthlike wrinkles form far away from the edge. The transition distance from uniaxial stress to biaxial stress is directly proportional to the film thickness [18,23]. For constrained liquid edge in this study, the stress anisotropy not only depends on the film thickness [see Fig. 3(a)], but also is significantly influenced by the width of the liquid stripe (see Supplemental Material Fig. S2 [13]). Furthermore, if the transition length of straight wrinkles is larger than the half width of silicone oil stripe, the stripe center usually forms herringbone or zigzag wrinkles by the competition of stress anisotropy and wrinkle history, as shown in Figs. 1(e) and 1(f). It is interesting that completely straight wrinkles across the entire stripe are rarely observed in the experiment. We note that the straight wrinkles at both edges separately propagate into the center and thus the frustration is unavoidable when they meet especially if the width of the stripe is not constant and the two edges are not parallel.

The researchers also investigated the wrinkle morphologies in constrained film regions on soft elastic substrates under isotropic compression. Choi *et al.* studied the wrinkle patterns in various film regions including circle, oval, stripe, square, hexagon, and triangle shapes [24]. Chan *et al.* studied the wrinkle evolution in a long film stripe with varied widths [23]. Zong *et al.* studied the photoisomerization-induced wrinkle evolution by dynamically tuning or selectively erasing partial wrinkles with visible light [25]. Huang *et al.* simulated the wrinkle morphologies in a circular region [26]. Ni *et al.* further simulated the wrinkle patterns in circular, square, and rectangular domains [27]. The experimental and theoretical results both showed that straight wrinkles are perpendicular to the edge while labyrinthlike or frustrationlike wrinkles form at

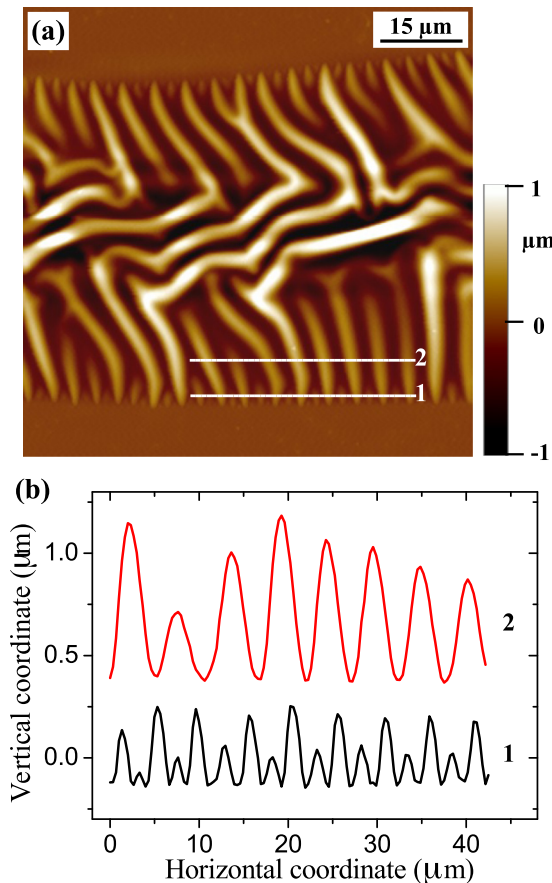


FIG. 4. Atomic force microscopy (AFM) image (a) and corresponding profiles (b) of hierarchical wrinkles in the iron film with  $h = 150$  nm.

the center, similar to our experimental observations. However, the wrinkle wavelengths on elastic foundations are always unchanged in the entire wrinkled region [23–27], which are in contrast to the hierarchical patterns in our experiment.

It should be noted here that hierarchical wrinkles can be observed in the films on soft elastic substrates with gradient of film thickness or substrate modulus [28,29]. But they are different from our experimental observations since the film thickness and substrate modulus are constant in our experiment. The thickness of the silicone oil substrate is also not a critical factor to affect the wavelengths of the wrinkles because the substrate thickness (several to tens micrometers) is much larger than the film thickness (several to 100 nanometers) in this study. Furthermore, although the previous studies showed that the wrinkles can evolve into localized delaminations by increasing compressive stress or film thickness [30,31], no obvious wrinkling-induced delamination was observed in our experiment.

On the other hand, similar hierarchical wrinkles have been extensively observed in free-sustained films or sheets including suspended curtains [32], meniscus of freestanding liquid crystal membranes [33], compressed polystyrene layers on water [34], graphenes on liquid copper [35], cobalt-chromium films on silicone oil [7], etc. It is clear that the liquid substrate or free interface plays a key role on the formation of hierarchical wrinkling near the edge. In the system of metal film on liquid stripe, the film edge is constrained by the strong adhesion between the metal film and the glass substrate. The edge constraint shows a similar boundary confinement reported in constrained sheet [32]. It leads to expansion restricted along the edge direction, resulting in the formation of wrinkles perpendicular to the edge. The hierarchical wrinkling results from the competition between bending energy of film, thermal expansion energy of substrate, and surface energy applied on the metal film from the metal-glass interface to metal-liquid interface, which will be discussed in detail in the next section. The previous studies also showed that the power exponent  $n$  is strongly dependent on the material property. The power exponent is close to  $2/3$  for short fabric and paper curtains and  $1/2$  for long fabric, rubber curtains, and graphene sheet [32,35]. For cobalt-chromium films on silicone oil, the power exponent is about 0.42 [7], which is very close to our experimental result ( $n \sim 0.46$ ).

### B. Wrinkling of thicker films after crack formation

It is now well known that as the deposition time (or film thickness) increases, the tensile stress of metal film increases accordingly owing to the thermal expansion of the underlying silicone oil substrate. When the tensile stress is beyond the breaking strength of the metal film, cracks form in the film, as shown in Fig. 5. The AFM images of film morphologies after crack occurrence are shown in Supplemental Material Fig. S3 [13]. The formation, morphology, and mechanism of the cracks will be discussed in the next section. After deposition, cooling of the system generates a compressive stress in the film, leading to the formation of wrinkle patterns. Because the occurrence of cracks will change the stress distribution in the film, the wrinkle patterns in cracked films are quite different from those in uncracked films. As shown in Fig. 5, the

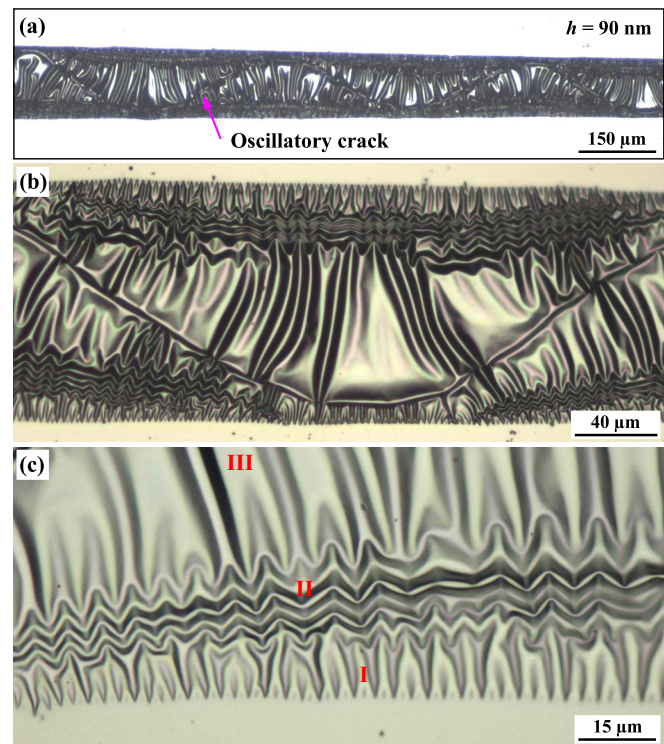


FIG. 5. Typical wrinkles of iron films on silicone oil stripes after formation of oscillatory cracks. Three distinct wrinkles including hierarchical (region I), wavy (region II), and straight (region III) structures can be seen clearly. The film thickness is  $h = 90$  nm.

wrinkle patterns in cracked films can be categorized into three distinct morphologies as follows. Hierarchical wrinkles form near the stripe edge (region I), similar to the morphologies of uncracked films. Straight wrinkles with large wavelengths form near the crack edge (region III). They are perpendicular to the crack due to the edge effect [18]. Wavy or herringbone wrinkles form in the region between the hierarchical and straight wrinkles (region II). Their main directions are always parallel to the stripe edge.

It is clear that the stripe edge is constrained by the strong adhesion of metal-glass interface while the crack edge is comparatively free due to the weak adhesion of metal-liquid interface. The cracked film piece is similar to a suspended curtain which has one constrained top edge and one free bottom edge [32]. The wrinkle wavelength increases gradually with increasing distance from constrained liquid edge, similar to the case of suspended curtains [32]. The compressive stress in suspended curtains is induced by gravity and it is uniaxial across the entire sample. Therefore the wrinkle patterns are always perpendicular to the constrained and free edges [32]. In our case, however, the compressive stress is uniform or isotropic in the film center. We suggest that the hierarchical wrinkles and straight wrinkles independently form at the constrained and free edges, respectively. When they propagate and meet together, the frustration occurs and wavy or herringbone wrinkles form.

Figure 6 shows the typical wrinkle patterns in iron films with varied thicknesses on wider silicone oil stripes after crack formation. We find that the sizes of both hierarchical

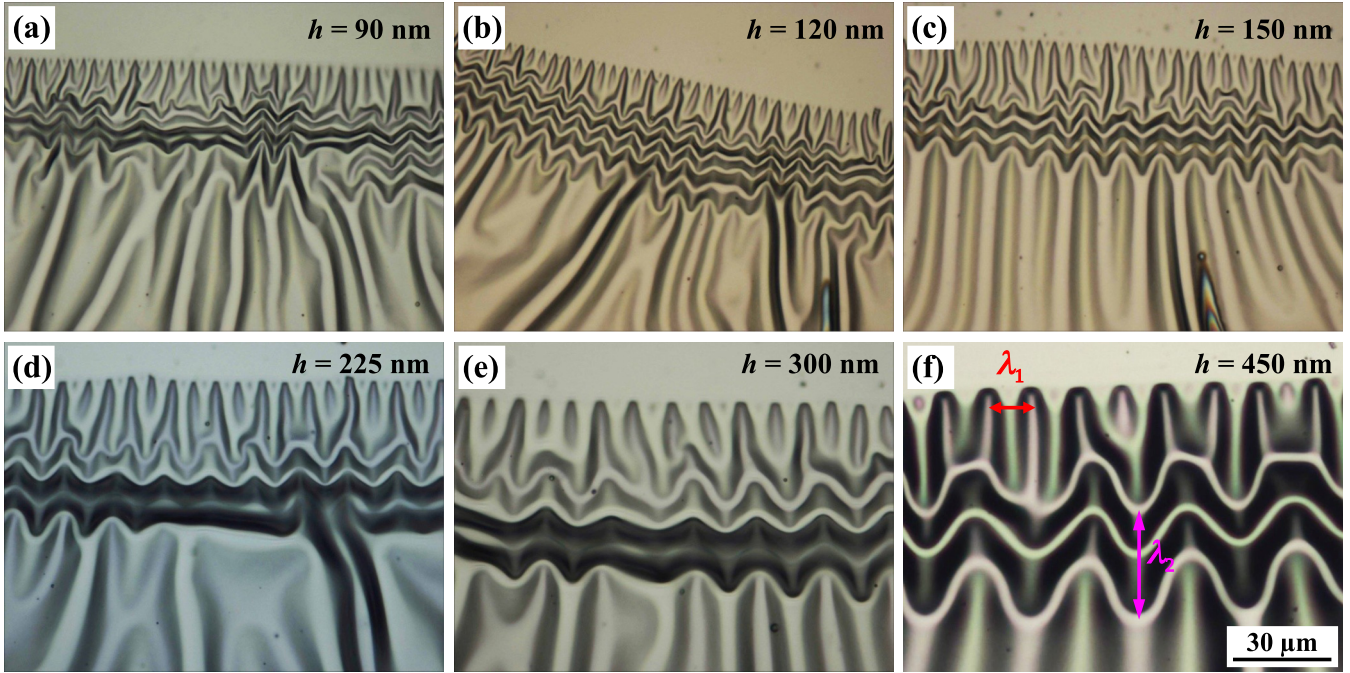


FIG. 6. Morphological evolution of wrinkle patterns with increasing iron film thickness for wider silicone oil stripes after crack formation. The wavelength of straight wrinkles near the stripe edge ( $x \sim 2.5 \mu\text{m}$ ) is denoted as  $\lambda_1$ . The wavelength of wavy wrinkles in region II is denoted as  $\lambda_2$ . All images have the same size of  $139 \times 104 \mu\text{m}^2$ .

and wavy wrinkles increase with increasing film thickness. The dependencies of the wavelength of hierarchical wrinkles (fixed at  $x \sim 2.5 \mu\text{m}$ )  $\lambda_1$  and wavelength of wavy wrinkles  $\lambda_2$  on the film thickness are shown in Fig. 7. The wavelengths of hierarchical wrinkles ( $x \sim 2.5 \mu\text{m}$ ) for uncracked films are also presented in Fig. 7(a). It is clear that the wavelengths of both hierarchical and wavy wrinkles increase with increasing film thickness.

A recent study discussed the energies of metal films deposited on liquid menisci. The total energy of the system can be expressed as [7]

$$U = U_B + U_G + U_{Th} + U_S, \quad (1)$$

where  $U_B$  is the bending energy of film,  $U_G$  is the gravitational energy of liquid,  $U_{Th}$  is the energy of the substrate due to thermal expansion mismatch,  $U_S$  is the additional stretching

energy in the metal film given by the metal-glass interface and metal-liquid interface. In such a system, the gravitational energy does not play a significant role, which is different from the cases of polymer films floating on fluids [34] and suspended curtains [32]. In the region near the constrained edge,  $U_B \sim D\lambda E_f h^3 \kappa^2$  with  $D$  the average distance over which the wrinkle wavelength  $\lambda$  is doubled,  $\kappa \sim A/\lambda^2$ ,  $A = \lambda\sqrt{\Delta}$  with  $\Delta$  the effective lateral compression imposed by the edge confinement according to the inextensibility hypothesis [35], the additional stretching energy  $U_S \sim T\epsilon_{\text{eff}}D\lambda$  with  $T$  the effective stretching stress along  $x$  axis, and  $\epsilon_{\text{eff}} \sim \lambda^2\Delta/D^2$  the effective elongation strain along the  $x$  axis [32]. These two energy terms in Eq. (1) become dominant and the total energy minimization in Eq. (1) with respect to  $D$  leads to  $D \sim \lambda^2$ . Furthermore, according to the formula  $d\lambda/dx = \lambda/D$  [32] we could derive  $\lambda(x) \sim x^{1/2}$ , in good agreement with our

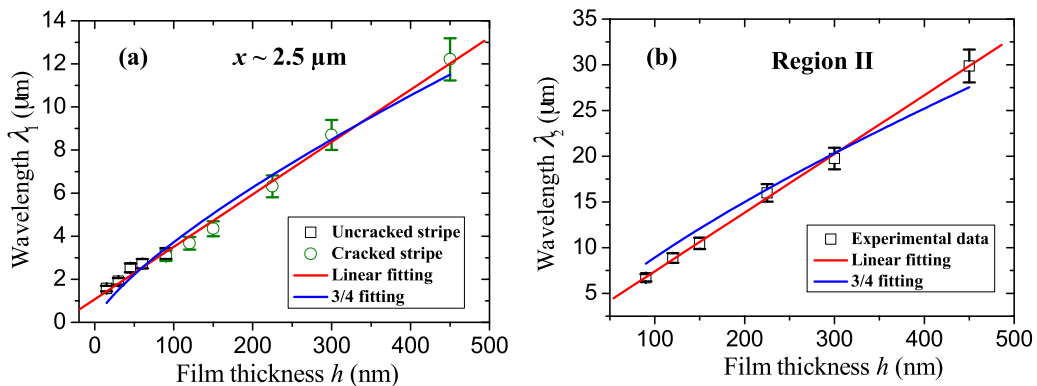


FIG. 7. Dependencies of the wrinkle wavelengths  $\lambda_1$  (a) and  $\lambda_2$  (b) on the film thickness  $h$ . The red and blue solid lines are linear and 3/4 fits to the experimental data, respectively.

experimental result ( $n \sim 0.46$ ). Such wrinkling hierarchy is similar to the result for the case of suspended heavy curtains [32], however the stretching stress in the current case may be caused by liquid meniscus instead of gravity.

In the region far away from the constrained edge, the additional stretching energy is very small and can be negligible [7]. Wrinkling of a thin film on a pure liquid substrate usually coarsens with time, inconsistent with the fact of the equilibrium wrinkling wavelength observed in our experiment. We rather assume that the silicon oil is viscoelastic. For a viscoelastic layer with a rubbery limit, the equivalent substrate elasticity may eventually stabilize the wrinkle and select its wavelength. Usually the energy change in the silicon oil supporting the thin film has the form  $U_{th} = \int_S \frac{1}{2} K \zeta^2 dS$  with  $\zeta$  defined as the out-of-plane deflection in the thin film [7,34]. On the one hand, when  $K = E_s/\lambda$  is assumed to be the effective stiffness of the silicon oil [7], the competition between the bending energy of film and deformation energy of the substrate  $U_{Th} \sim D\lambda E_s A^2/\lambda$  leads to an equilibrium wrinkle wavelength, the same as the case of films resting on elastic substrates [18–29]. Such equilibrium wavelength can be expressed as

$$\lambda = 2\pi h \left( \frac{E_f(1 - \nu_s^2)}{3E_s(1 - \nu_f^2)} \right)^{1/3}. \quad (2)$$

On the other hand, when  $K = \rho g$  is assumed to be the effective stiffness of the silicon oil, the selected wavelength would be  $\lambda \propto h^{3/4}$  [34]. As a rough estimation, we cannot identify the exact energy change in the silicon oil supporting the thin film. In Fig. 7, we found that there is no significant difference between  $\lambda \propto h$  and  $\lambda \propto h^{3/4}$  to fit the experimental data. Furthermore, the equivalent modulus of silicone oil can be estimated by using Eq. (2) when the film thickness is much small (e.g.,  $h < 90$  nm) and the surface modification during deposition can be negligible. Based on the saturated wrinkle wavelengths (at stripe center) shown in Fig. 2, the equivalent modulus of silicone oil is thus estimated to be about 0.5 MPa.

Figure 8 shows the morphological evolution of wrinkle patterns with increasing film thickness for narrower silicone oil stripes after crack formation. We find that the hierarchical wrinkling near the stripe edge disappears for thicker films. Furthermore, the wavy or herringbone wrinkles evolve into arcuate wrinkles. The wrinkle wavelength increases with increasing film thickness, which can be well explained by Eq. (2). We suggest that the silicone oil stripes with smaller widths can be modified easily to form a polymer layer atop [7,8], leading to the decrease of surface energy and disappearance of hierarchical wrinkling.

### C. Oscillatory cracks

It can be seen from Figs. 5 and 8 that the cracks on the silicone oil stripes are oscillatory. Their shapes are not exact sine functions, but are sawtoothlike and asymmetric. Figure 8 shows that the morphology and number of oscillatory cracks are independent of the film thickness. As we have discussed above, the cracks are driven by the tensile stress during the film deposition. The liquid oil interlayer between the metal film and glass surface with low interface toughness can trap

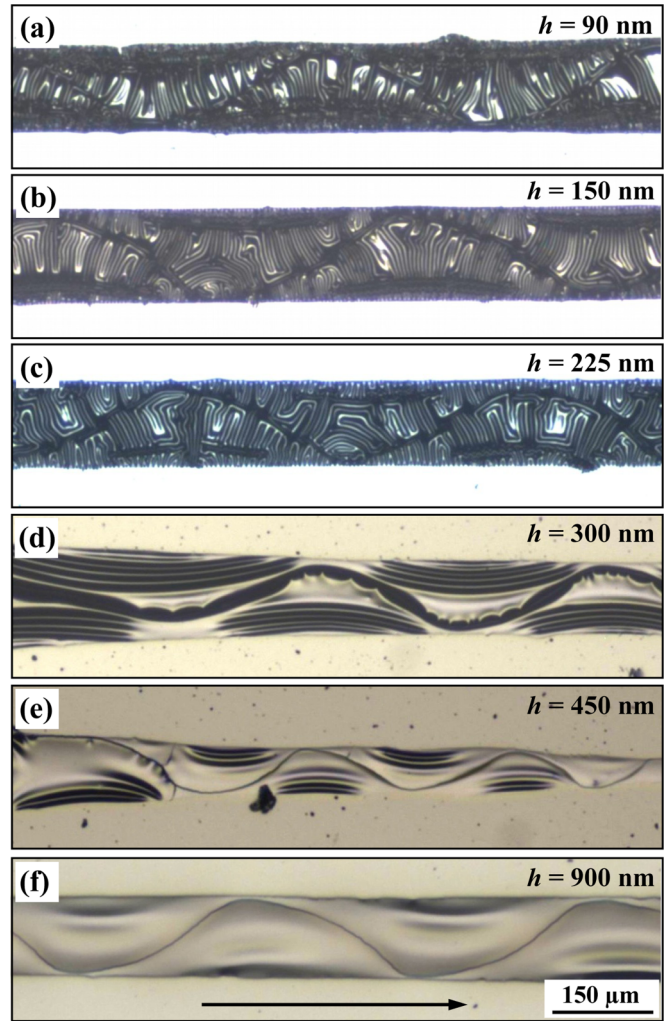


FIG. 8. Morphological evolution of wrinkle patterns with increasing iron film thickness for narrower silicone oil stripes after crack formation. The black arrow in (f) denotes the propagation directions of the oscillatory cracks. All images have the same size of  $1000 \times 200 \mu\text{m}^2$ .

the crack at the interface and thus the crack extending in the film does not dip into the substrate. In such a case, Griffith's equation can be adapted to analyze the film cracking behavior. According to the Griffith classical criterion, a channel crack with possible interface sliding propagates when the released elastic energy overcomes the fracture energy, i.e.,  $2\gamma h e \geq G_c h$  with  $e = h\sigma^2(1 - \nu)/E_f$  [36–38]. Here  $e$  is the elastic energy density,  $G_c$  is the fracture energy density,  $\sigma$  is the tensile stress,  $\gamma$  is a coefficient that characterizes the confinement effect in the film imposed by the substrate.  $\gamma$  can be very large when the substrate is more compliant or the interlayer slides or creeps in shear. The above equation can be rewritten as

$$h \geq \frac{G_c E_f}{2\gamma(1 - \nu)\sigma^2}. \quad (3)$$

It indicates that the cracks initiate beyond a critical film thickness expressed as  $h_c = G_c E_f / 2\gamma(1 - \nu)\sigma^2$ , which has been verified by many experimental observations [38–40].

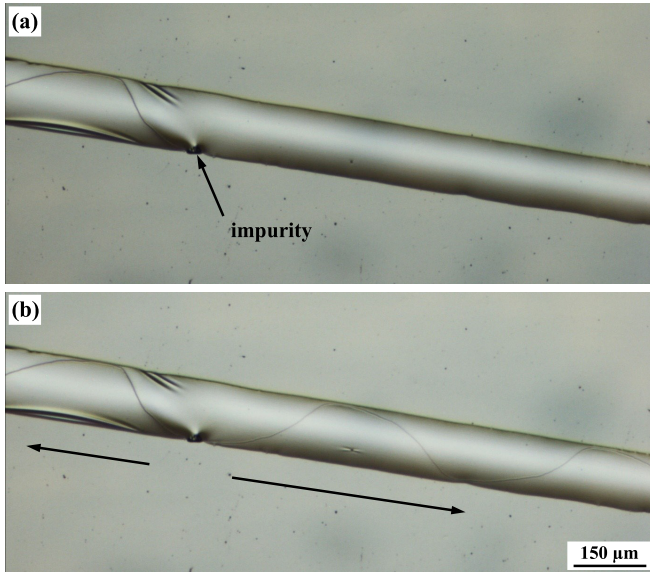


FIG. 9. *In situ* propagation of an oscillatory crack by heating the sample to 200 °C. The black arrows in (b) denote the propagation directions of the crack starting from an impurity point. The film material is titanium. Both images have the same size of  $1390 \times 600 \mu\text{m}^2$ .

In our experiment, the oscillatory cracks are always limited to the silicone oil stripes and the metal films on glass surfaces remain crack free, which can be attributed to the following two reasons. First, the tensile stress of the film on silicone oil stripes is much larger than that on glass surfaces due to the large thermal expansion coefficient of the silicone oil. Larger stress leads to smaller critical thickness according to Eq. (3). Second, the coefficient  $\gamma$  can be much larger for compliant substrates compared with the rigid substrates [41]. The increase of coefficient  $\gamma$  is equivalent to the decrease of fracture toughness of the film ( $\sim G_c/\gamma$ ) as discussed in the literature [42]. Our experiment also shows that the critical thicknesses for various metal films on silicone oil stripes are different. They are about 15, 15, 60, 90, and 120 nm for copper, cobalt, nickel, iron, and titanium films, respectively. On the other hand, because the interfacial adhesion between the metal film and liquid substrate is very weak, the film pieces can freely move on the liquid surface after crack formation [9–12]. It is unnecessary to form new cracks to release the increased tensile stress in this case and thus the crack number is unchanged as the film thickness increases.

To further understand the formation of such oscillatory crack pattern, we performed a simple test to detect the *in situ* propagation of the crack by external heating. First a heater was placed under the optical microscope and a film sample with critical thickness (some stripes have formed cracks and some not) was placed on the heater. The optical microscope was focused on an uncracked stripe. Then the temperature of the heater was increased to 200 °C gradually. The morphological evolution of the film was investigated by the optical microscope, as shown in Fig. 9. It is clear that the oscillatory crack nucleates at a film impurity and then propagates towards the opposite directions as denoted by the black arrows in Fig. 9(b). When the crack approaches the stripe edge, the

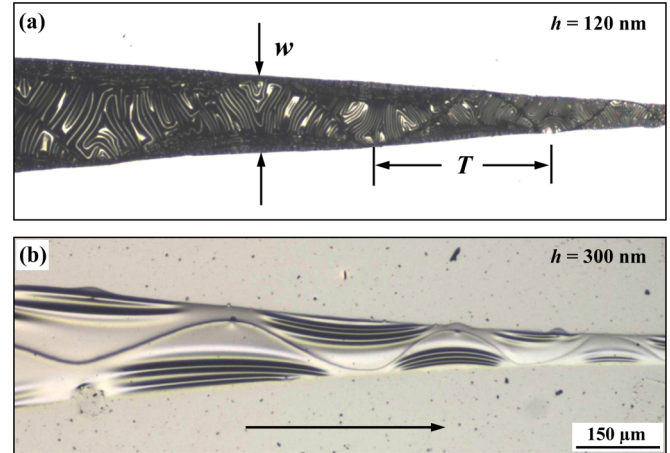


FIG. 10. Oscillatory cracks on two tapered silicone oil stripes with different iron film thicknesses. The crack period and stripe width are denoted as  $T$  and  $w$ , respectively. The black arrow in (b) denotes the propagation directions of the cracks. Both images have the same size of  $1200 \times 400 \mu\text{m}^2$ .

angle between the crack and stripe edge is comparatively large. Then the crack deviates from the edge gradually and the angle between the crack and stripe edge is very small. Because of the asymmetry of the crack trajectory when approaching to and detaching from the stripe edge, the crack shapes are not exact sine functions, but are sawtoothlike. This feature can help us to distinguish the propagation direction of the oscillatory crack conveniently. Note that all the oscillatory cracks shown in Fig. 8 propagate from left to right, as denoted by the black arrow in Fig. 8(f).

Figure 10 shows the oscillatory cracks on two tapered silicone oil stripes with different film thicknesses. The wrinkle morphologies as those shown in Fig. 8 are clearly observed here. It can be concluded that the oscillatory cracks on tapered stripes always propagate from the wider ends to narrower ends, as denoted by the black arrow in Fig. 10(b). Furthermore, the crack period decreases with decreasing stripe width. To further understand the scaling law of the oscillatory crack, we measured the dependence of the crack period  $T$  on the stripe width (or crack amplitude)  $w$  for varied film thicknesses, as shown in Fig. 11(a). It is clear that the crack period is in direct proportion to the stripe width, independent of the film thickness. The linear slope (i.e., the ratio of period to amplitude) is about 3.7. We also prepared various metal (including iron, copper, nickel, titanium, and cobalt) films on the silicone oil stripes. It is found that the oscillatory cracks in different metal films are quite similar, as shown in Supplemental Material Fig. S4 [13]. The crack period is also proportional to the stripe width for all the metal materials, independent of the film thickness, as shown in Supplemental Material Fig. S5 [13]. Furthermore, the linear slopes for different materials are all equal to about 3.7, as shown in Fig. 11(b).

These results indicate that the feature of the oscillatory crack is independent of the film material and film thickness as well as other experimental conditions. It is crucially dependent on the geometrical feature of a brittle film resting on a liquid stripe under tension. To verify the universality of the oscillatory crack in similar structural system, we prepared

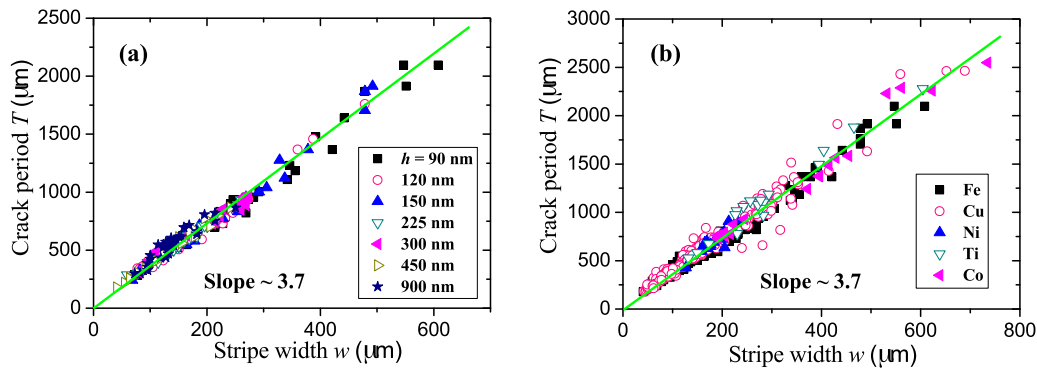


FIG. 11. (a) Dependence of the crack period  $T$  on the stripe width  $w$  for varied film thicknesses. (b) Dependence of the crack period  $T$  on the stripe width  $w$  for different film materials. The solid lines are linear fits to the experimental data.

iron films on soft elastic PDMS stripes. It shows that similar oscillatory cracks can form on the PDMS stripes, as shown in Fig. 12. The formation of localized wrinkles near the oscillatory crack is due to the plastic deformation of metal film induced by a high stress of crack tip [39]. Our experiment shows that the localized wrinkles are usually prominent in iron films on PDMS stripes (see Fig. 12) but are not obvious on silicone oil stripes (see Figs. 8–10), which can be attributed to the following two reasons. First, the iron films on PDMS stripes are wrinkle-free except for the plastic deformation region, while the films on silicone oil stripes are entirely wrinkled. Second, the plastic deformation region of the film on silicone oil is wider than that on PDMS due to the very soft feature of liquid. The trace of plastic deformation region of the iron films on silicone oil stripes can be occasionally observed in experiment, as shown in Supplemental Material Fig. S6 [13]. It should be noted here that the formation window of oscillatory cracks on PDMS stripes is comparatively narrow compared to that on liquid stripes. When the film thickness or stripe width increases, more cracks form in the film due to the strong adhesion of metal-PDMS interface, leading to the formation of irregular crack network, as shown in Supplemental Material Fig. S7 [13].

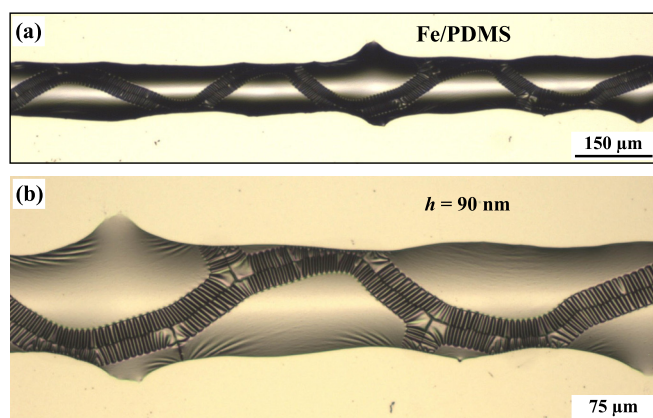


FIG. 12. Oscillatory cracks in iron films deposited on PDMS stripes. Note that the localized straight wrinkles near the crack are induced by the localized plastic deformation of metal film during the propagation of crack.

Periodic cracks with peculiar shapes have been investigated in various film systems. Straight, oscillatory, and branched cracks can form in quenched glass or silicon plates driven by a gradient thermal stress [43,44]. When a biaxially strained thin rubber sheet is pierced by a moving object, oscillatory or cycloidal tear morphologies form behind the object [45,46]. When the brittle films on crystallized substrates are annealed at high temperature, the cracks can penetrate deeply into the substrate, leading to periodically oscillatory crack paths along specific orientations [47]. Various self-replicated crack patterns including crescent alleys, spirals, and parallel bands have been observed in thin sol-gel films, where crack propagation and interface delamination occur simultaneously [37,41,48]. Microscale wavy crack propagation has been observed in silicon nitride films deposited on patterned metal, polymer, and graphene lines through a simple heating process [42,49].

Our experiment system is similar to the cases of brittle films on patterned substrates with prefabricated heterogeneous lines [42,49] since the silicone oil stripe can be regarded as an interlayer between the metal film and glass surface. Such a system can be treated as a two-dimensional (2D) projection of a brittle adhesive joint, where a brittle medium (adhesive) is sandwiched between two rigid materials [50,51]. Oscillatory cracks can be observed in the brittle adhesive joints and have been widely investigated experimentally and theoretically [50,51]. It is found that the crack period is three to four times the adhesive thickness (i.e., stripe width in this study), in good agreement with our experiment. In the case of silicon nitride films on metal lines, the relation between crack period and stripe width can be written as  $T = 2.46w + C$ , where  $C$  is a constant [49]. In literature [42], the relation between crack period and stripe width can be written as  $T = 1.93w + 43$ . In our experiment, the crack period is strictly proportional to the stripe width, which can be expressed as  $T \approx 3.7w$ . The difference of the scaling between our experiment and the literature is mainly due to the property of interlayer. The silicone oil interlayer in this study is much softer than metal materials used in literature [42,49]. Our experiment system is closer to the brittle adhesive joint since the adhesive is very soft compared to the rigid materials. Furthermore, the previous study showed that cracks initiate only when the interlayer is softer than the film [42].

It is clear that the liquid interlayers in this study have a significant advantage compared to traditional solid (metal,

semiconductor, graphene, etc.) interlayers [42,49]. Various complex but ordered liquid or soft polymer interlayer arrays (including 2D and 3D configurations) can be easily achieved by direct ink writing or other printing methods [52]. No expensive equipment and multistep preparation processes are needed here. We believe that this technique can be developed to fabricate multiple controllable surface patterns by constructing various thin films (or sheets) on prefabricated liquid or soft polymer interlayer arrays.

#### IV. CONCLUSIONS

In summary, coexisting hierarchical wrinkles and oscillatory cracks in metal films deposited on silicone oil stripes have been described and discussed in detail. It is found that a high tensile stress is built up in the metal film due to the thermal expansion of the underlying liquid substrate, which is relieved by formation of oscillatory cracks with sawtoothlike shapes and asymmetric features. The ratio of crack period to amplitude is a constant of  $\sim 3.7$ , independent of the stripe width and film material. The formation of oscillatory cracks is attributed to the constrained edges and uniform tensile stress, similar to the case of “brittle adhesive joints.” After deposition, the compressive stress in the film generates various wrinkle patterns, depending on the stripe width, film

thickness, and crack shape. For uncracked films, hierarchical wrinkles with changing wavelengths form near the stripe edge while labyrinth wrinkles form at the center. For cracked films, three distinct wrinkles including hierarchical, wavy (or herringbone), and straight structures can be observed. The formation of complex wrinkles in cracked films is attributed to the constrained (or free) edge effect and stress anisotropy. This work can provide a deep insight into the formations of ordered wrinkle and crack patterns in constrained film structures on liquid substrates. The technique to harness multiple stress-driven patterns by prefabricating liquid (or soft polymer) interlayer structures should be beneficial for a wide range of practical applications.

#### ACKNOWLEDGMENTS

This work was supported by the National Natural Science Foundation of China (Grants No. 11204283, No. 11104054, No. 11672285) and the Strategic Priority Research Program of the Chinese Academy of Sciences (Grant No. XDB22040502), the Collaborative Innovation Center of Suzhou Nano Science and Technology, and the Fundamental Research Funds for the Central Universities (Grant No. WK2090050043).

- 
- [1] J. Huang, M. Juskiewicz, W. H. de Jeu, E. Cerda, T. Emrick, N. Menon, and T. P. Russell, *Science* **317**, 650 (2007).
- [2] L. Pociavsek, R. Dellsy, A. Kern, S. Johnson, B. Lin, K. Y. C. Lee, and E. Cerda, *Science* **320**, 912 (2008).
- [3] D. P. Holmes and A. J. Crosby, *Phys. Rev. Lett.* **105**, 038303 (2010).
- [4] H. King, R. D. Schroll, B. Davidovitch, and N. Menon, *Proc. Natl. Acad. Sci. USA* **109**, 9716 (2012).
- [5] J. D. Paulsen, V. Démery, K. B. Toga, Z. Qiu, T. P. Russell, B. Davidovitch, and N. Menon, *Phys. Rev. Lett.* **118**, 048004 (2017).
- [6] X. Liu and M. Wuttig, *Phys. Rev. B* **73**, 033405 (2006).
- [7] S. Deng and V. Berry, *ACS Appl. Mater. Interfaces* **8**, 24956 (2016).
- [8] S. J. Yu, Y. J. Zhang, H. Zhou, M. G. Chen, X. F. Zhang, Z. W. Jiao, and P. Z. Si, *Phys. Rev. E* **88**, 042401 (2013).
- [9] P. Cai, S. Yu, X. Xu, M. Chen, C. Sui, and G. X. Ye, *Appl. Surf. Sci.* **255**, 8352 (2009).
- [10] S. J. Yu, Y. J. Zhang, Q. L. Ye, P. G. Cai, X. W. Tang, and G. X. Ye, *Phys. Rev. B* **68**, 193403 (2003).
- [11] M. G. Chen, J. P. Xie, and G. X. Ye, *Phys. Lett. A* **360**, 323 (2006).
- [12] D. Vella and J. S. Wettlaufer, *Phys. Rev. Lett.* **98**, 088303 (2007).
- [13] See Supplemental Material at <http://link.aps.org/supplemental/10.1103/PhysRevE.99.062802> for details about the sectional profiles of silicone oil stripes, wrinkle morphologies on a tapered silicone oil stripe, morphologies and sizes of oscillatory cracks, and localized wrinkles induced by crack-tip plastic deformation. Seven supplemental figures are provided.
- [14] G. X. Ye, T. Michely, V. Weidenhof, I. Friedrich, and M. Wuttig, *Phys. Rev. Lett.* **81**, 622 (1998).
- [15] T. Ohzono, H. Monobe, N. Fukuda, M. Fujiwara, and Y. Shimizu, *Small* **7**, 506 (2011).
- [16] T. Torimoto, K. Okazaki, T. Kiyama, K. Hirahara, N. Tanaka, and S. Kuwabata, *Appl. Phys. Lett.* **89**, 243117 (2006).
- [17] S. Yu, Y. Sun, S. Li, and Y. Ni, *Soft Matter* **14**, 6745 (2018).
- [18] N. Bowden, S. Brittain, A. G. Evans, J. W. Hutchinson, and G. M. Whitesides, *Nature (London)* **393**, 146 (1998).
- [19] J. Rodríguez-Hernández, *Prog. Polym. Sci.* **42**, 1 (2015).
- [20] J. Wang, B. Li, Y. P. Cao, X. Q. Feng, and H. Gao, *Appl. Phys. Lett.* **108**, 021903 (2016).
- [21] B. J. Gurmessa and A. B. Croll, *Soft Matter* **13**, 1764 (2017).
- [22] Y. Sun, L. Yan, C. Li, and B. Chen, *Eur. Phys. J. E* **41**, 31 (2018).
- [23] E. P. Chan and A. J. Crosby, *Soft Matter* **2**, 324 (2006).
- [24] W. M. Choi, J. Song, D. Y. Khang, H. Jiang, Y. Y. Huang, and J. A. Rogers, *Nano Lett.* **7**, 1655 (2007).
- [25] C. Zong, Y. Zhao, H. Ji, X. Han, J. Xie, J. Wang, Y. Cao, S. Jiang, and C. Lu, *Angew. Chem. Int. Ed.* **55**, 3931 (2016).
- [26] Z. Y. Huang, W. Hong, and Z. Suo, *J. Mech. Phys. Solids* **53**, 2101 (2005).
- [27] Y. Ni, L. He, and Q. Liu, *Phys. Rev. E* **84**, 051604 (2011).
- [28] Y. Ni, D. Yang, and L. He, *Phys. Rev. E* **86**, 031604 (2012).
- [29] S. Yu, Y. Ni, L. He, and Q. L. Ye, *ACS Appl. Mater. Interfaces* **7**, 5160 (2015).
- [30] K. Pan, Y. Ni, L. He, and R. Huang, *Int. J. Solids Struct.* **51**, 3715 (2014).
- [31] A. J. Nolte, J. Y. Chung, C. S. Davis, and C. M. Stafford, *Soft Matter* **13**, 7930 (2017).
- [32] H. Vandeparre, M. Piñeirua, F. Brau, B. Roman, J. Bico, C. Gay, W. Bao, C. N. Lau, P. M. Reis, and P. Damman, *Phys. Rev. Lett.* **106**, 224301 (2011).
- [33] J. C. Loudet, P. V. Dolganov, P. Patrício, H. Saadaoui, and P. Cluzeau, *Phys. Rev. Lett.* **106**, 117802 (2011).

- [34] J. Huang, B. Davidovitch, C. D. Santangelo, T. P. Russell, and N. Menon, *Phys. Rev. Lett.* **105**, 038302 (2010).
- [35] L. Meng, Y. Su, D. Geng, G. Yu, Y. Liu, R. F. Dou, J. C. Nie, and L. He, *Appl. Phys. Lett.* **103**, 251610 (2013).
- [36] M. R. Begley and J. W. Hutchinson, *The Mechanics and Reliability of Films, Multilayers and Coatings* (Cambridge University Press, Cambridge, UK, 2017).
- [37] J. Marthelot, B. Roman, J. Bico, J. Teisseire, D. Dalmas, and F. Melo, *Phys. Rev. Lett.* **113**, 085502 (2014).
- [38] E. J. Kappert, D. Pavlenko, J. Malzbender, A. Nijmeijer, N. E. Benes, and P. A. Tsai, *Soft Matter* **11**, 882 (2015).
- [39] S. Yu, X. Zhang, X. Xiao, H. Zhou, and M. Chen, *Soft Matter* **11**, 2203 (2015).
- [40] R. Seghir and S. Arscott, *Sci. Rep.* **5**, 14787 (2015).
- [41] J. Marthelot, J. Bico, F. Melo, and B. Roman, *J. Mech. Phys. Solids* **84**, 214 (2015).
- [42] M. R. Cho, J. H. Jung, M. key Seo, S. U. Cho, Y. D. Kim, J. H. Lee, Y. S. Kim, J. Hone, J. Ihm, and Y. D. Park, *Sci. Rep.* **7**, 43400 (2017).
- [43] A. Yuse and M. Sano, *Nature (London)* **362**, 329 (1993).
- [44] R. D. Deegan, S. Chheda, L. Patel, M. Marder, H. L. Swinney, J. Kim, and A. de Lozanne, *Phys. Rev. E* **67**, 066209 (2003).
- [45] A. Ghatak and L. Mahadevan, *Phys. Rev. Lett.* **91**, 215507 (2003).
- [46] B. Audoly, P. M. Reis, and B. Roman, *Phys. Rev. Lett.* **95**, 025502 (2005).
- [47] K. H. Nam, I. H. Park, and S. H. Ko, *Nature (London)* **485**, 221 (2012).
- [48] N. Wan, J. Xu, T. Lin, L. Xu, and K. Chen, *Phys. Rev. B* **80**, 014121 (2009).
- [49] D. Kim, P. Makaram, and C. V. Thompson, *Appl. Phys. Lett.* **97**, 071902 (2010).
- [50] A. R. Akisanya and N. A. Fleck, *Int. J. Fracture* **58**, 93 (1992).
- [51] B. Chen and D. A. Dillard, *Int. J. Solids Struct.* **38**, 6907 (2001).
- [52] Y. Kim, H. Yuk, R. Zhao, S. A. Chester, and X. Zhao, *Nature (London)* **558**, 274 (2018).